International Journal of Heat and Mass Transfer 52 (2009) 5712–5718

Contents lists available at ScienceDirect

International Journal of Heat and Mass Transfer

journal homepage: www.elsevier.com/locate/ijhmt

Convective flow and heat transfer in a tall porous cavity side-cooled with temperature profile

Ridha Ben Yedder *, Fouad Erchiqui

Unité d'enseignement et de recherche en sciences appliquées, Université de Québec en Abitibi-Témescamingue, 445 boul. de l'Université, Rouyn-Noranda (PQ), Canada J9X 5E4

ARTICLE INFO

Article history:
Received 30 May 2009
Received in revised form 26 August 2009
Available online 18 September 2009

Keywords:
Numerical simulation
Natural convection
Porous media
Non-uniform heating
Tall cavity

ABSTRACT

Natural convection in an air-filled (*Prandtl* number = 0.7) porous cavity with profiled side cooling and constant bottom heating is investigated over the *Rayleigh* number range of 1×10^4 to 1×10^8 at two *Darcy* numbers: 1×10^{-4} and 1×10^{-6}. The aspect ratio based on cavity height was varied from 0.5 to 0.1 to investigate penetration length according to linear or sinusoidal temperature profile. The general non-Darcy model adopted in this work was validated against experimental and theoretical results in the literature and *Nusselt* number was predicted within less than 3% in the worst case. The effect of left wall imposed temperature profile was investigated in detail. Different convective regimes were observed depending on the imposed profile. An active region was found to take place with the linear temperature profile and with extent proportional to *Rayleigh* number as predicted by scale analysis.

1. Introduction

Flow and heat transfer in porous media has been extensively modeled due to the wide variety of applications in areas such as geothermal systems, the petroleum industry and metal processing. A comprehensive literature review is provided in [1,2]. Early numerical studies were based on the Darcy model due to the relative ease of solving the resulting equations for conservation of momentum. However, the Darcy law applies only to slow flows and does not account for inertial and boundary effects (known as non-Darcy effects) which become important in practical situations where flow velocity is relatively high or a boundary is present. Vafai and Tien [3] provide a detailed discussion on these non-Darcian effects.

Recent studies have considered other effects such as the variable porosity in Nithiarasu et al. [4] and radiation and non-equilibrium models in Badruddin et al. [5].

Another research stream addresses flow and heat transfer induced by a vertical cylinder immersed in a porous medium. Minkowycz and Cheng [6] analyzed natural convective flow around a vertical cylinder embedded in a saturated porous medium, where cylinder surface temperature is a power function of cylinder height. They obtained exact and approximate solutions using boundary-layer approximations. Vasantha and Nath [7] used an extended perturbation series method to obtain a numerical solution for the thermal boundary-layer along an isothermal cylinder in a porous medium. Bejan [8,9], from his analysis of natural convection in a vertical cylindrical well filled with a porous medium, pointed out that an important feature of similarity flow is that the depth to which the free-convection pattern penetrates the well is proportional to the temperature difference driving the flow.

To qualitatively measure the flow front penetration, Manca and Nardini [10] experimentally studied convective cell development in an open horizontal cavity and showed that its strength is proportional to *Ra*.

Profiled heating in rectangular fluid-filled cavity has been investigated by Ben Yedder and Bilgen [11] and Poulikakos [12], among others, demonstrating the effect of *Ra* on penetration length. Recently, Sathiyamoorthy et al. [13] investigated non-uniform heating of a porous cavity without considering the effect of aspect ratio or the temperature profile on the side boundary. This suggests that the knowledge of flow characteristics in such configurations remains incomplete: multi-cellular flow, stagnant regions and penetration length are all closely related to the imposed profile boundary temperature.

The above studies suggest that the extent of the main active convective cell is proportional to the temperature difference driving the flow. The aim of this work is to clarify the effect of boundary conditions on flow in a tall porous cavity using the Brinkman-extended Darcy equations of motion, including convective terms. Few studies have addressed the effect of profiled cooling on flow and heat transfer characteristics in porous cavities with variable aspect ratio. Moreover, the model can be directly applied to optimize fuel cells, where heat front propagation is a major concern, and to geothermal layers where a good estimation of fluid penetration length is important.

* Corresponding author. Tel.: +1 514 321 5660; fax: +1 514 321 4150.
E-mail address: ridha.benyedder@uqat.ca (R.B. Yedder).

0017-9310/$ - see front matter © 2009 Elsevier Ltd. All rights reserved.
doi:10.1016/j.ijheatmasstransfer.2009.08.016

Nomenclature

A	half-cavity aspect ratio, = $L/2H$
c_p	heat capacity, J/kg K
g	acceleration due to gravity, m/s^2
h	penetration length, m
H	cavity height, m
k	thermal conductivity, W/m K
K	medium permeability
L	cavity width, m
Nu	Nusselt number, Eq. (13)
p'	pressure, Pa
p	dimensionless pressure, $= (p' - p'_\infty)H^2/\rho\alpha^2$
Pr	Prandtl number, $= \nu/\alpha$
Ra	Rayleigh number, $= g\beta\Delta TH^3/(\nu\alpha)$
t'	time, s
T	temperature, K
ΔT	temperature difference, $= T_h - T_c$, K
u, v	dimensionless Darcy velocities, $= u'H/\alpha, v'H/\alpha$
x, y	dimensionless Cartesian coordinates, = $x'/H, y'/H$
x', y'	Cartesian coordinates

Greek symbols

α	diffusivity, m^2/s
β	volumetric coefficient of thermal expansion, 1/K
ϵ	porosity
ν	kinematic viscosity, m^2/s
ρ	fluid density, kg/m^3
ψ	stream function
θ	dimensionless temperature, = $(T - T_c)/\Delta T$
t	dimensionless time, $\alpha t'/H^2$

Superscripts

-	average
$'$	dimensional values
$*$	modified numbers

Subscripts

a	air
c	cold, ambient value
h	hot, active
loc	local
max	maximum
min	minimum

2. Mathematical model

The problem under study is depicted in Fig. 1. Temperature profiles are imposed along the left and right walls and the bottom wall is maintained at a constant, higher temperature. This temperature difference drives a Bénard type flow. The extent and topology of the flow depends on the imposed temperature gradient. In this study, two temperature profiles are considered:

$$\left.\begin{aligned} T(y') &= T_c + \Delta T \cos\left(\tfrac{\pi}{2}\tfrac{y'}{H}\right) \\ T(y') &= T_c + \Delta T\left(1 - \tfrac{y'}{H}\right) \end{aligned}\right\} \quad (1)$$

For purposes of this study, the following assumptions were made: the flow is a two-dimensional, laminar and incompressible Newtonian fluid, with no viscous dissipation. Gravity acts in the vertical direction, porous properties are constant, density variations are ignored – except in the buoyancy term (the Boussinesq approximation) – and radiation heat exchange is negligible.

The governing equations are based on the Darcy–Brinkman model (see [4]).

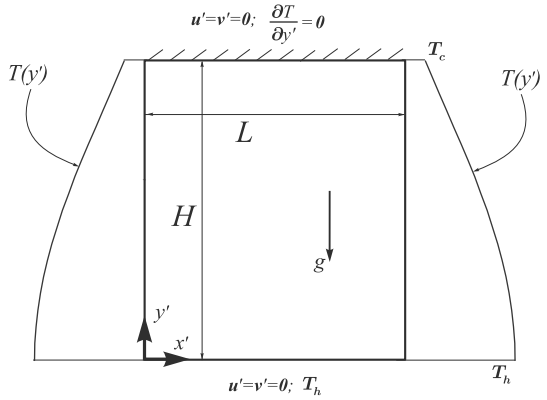

Fig. 1. Problem under study.

$$\frac{\partial u'}{\partial x'} + \frac{\partial v'}{\partial y'} = 0 \quad (2)$$

$$\frac{\partial u'}{\partial t'} + u'\frac{\partial u'}{\partial x'} + v'\frac{\partial u'}{\partial y'} = -\frac{1}{\rho}\frac{\partial p'}{\partial x'} + \nu\nabla^2 u' - \frac{\nu}{K}u' \quad (3)$$

$$\frac{\partial v'}{\partial t'} + u'\frac{\partial v'}{\partial x'} + v'\frac{\partial v'}{\partial y'} = -\frac{1}{\rho}\frac{\partial p'}{\partial y'} + \nu\nabla^2 v' + g\beta(T - T_c) - \frac{\nu}{K}v' \quad (4)$$

$$\frac{\partial T}{\partial t'} + u'\frac{\partial T}{\partial x'} + v'\frac{\partial T}{\partial y'} = \alpha\nabla^2 T \quad (5)$$

In non-dimensional form, and following the dimensionless quantities provided in the nomenclature, these equations become:

$$\frac{\partial u}{\partial x} + \frac{\partial v}{\partial y} = 0 \quad (6)$$

$$\frac{\partial u}{\partial t} + u\frac{\partial u}{\partial x} + v\frac{\partial u}{\partial y} = -\frac{\partial p}{\partial x} + Pr\nabla^2 u - \frac{Pr}{Da}u \quad (7)$$

$$\frac{\partial v}{\partial t} + u\frac{\partial v}{\partial x} + v\frac{\partial v}{\partial y} = -\frac{\partial p}{\partial y} + Pr\nabla^2 v + RaPr\theta - \frac{Pr}{Da}v \quad (8)$$

$$\frac{\partial \theta}{\partial t} + u\frac{\partial \theta}{\partial x} + v\frac{\partial \theta}{\partial y} = \nabla^2\theta \quad (9)$$

This produces the following dimensionless numbers - that characterize convective flow in porous media:

$$Ra = \frac{g\beta\Delta TH^3}{\nu\alpha} \quad Pr = \frac{\nu}{\alpha} \quad Da = \frac{K}{H^2} \quad (10)$$

Considering the above-made assumptions and because the problem is symmetric, the governing equations are solved on only half the domain, with the following non-dimensional boundary conditions:

$$\left.\begin{array}{lll} \text{On all solid boundaries :} & & u = v = 0 \\ \text{On the symmetric plane :} & x = A & u = 0, \frac{\partial v}{\partial x} = 0, \frac{\partial \theta}{\partial x} = 0 \\ \text{On } x = 0; & 0 < y < 1 & \theta = \theta(y) \\ \text{On } y = 0; & 0 < x < A & \theta = 1 \\ \text{On } y = 1; & 0 < x < A & \frac{\partial \theta}{\partial y} = 0 \end{array}\right\} \quad (11)$$

3. Numerical procedure and validation

The SIMPLER (Semi-Implicit Method for Pressure Linked Equations Revised) algorithm [14] is used to solve Eqs. (6)–(9). The discretized equation system, using the hybrid interpolation scheme for the advection term, is iterated in time until a steady state solution is obtained:

$$\sum(\phi_{ij} - \phi_{ij}^{old}) \leqslant 10^{-4} \quad (12)$$

where ϕ stands for the dependent variables u, v and θ.

The computer code based on the above-presented mathematical equations was validated earlier [11,15] for the benchmark case of a differentially heated cavity [16] and will not be repeated here. Validation of the porous media case is also compared against [4,17,18] for different porosity values ϵ.

The results obtained with the modified model are consistent with those of [4] (see Table 1) which, for validation purposes, ignored the non-linear drag term in the momentum equations, and hence used the same model as above. Table 2 compares the *Nu* number for the case where $\epsilon = 1.0$. The differences, albeit within less than 3%, are greater for high *Ra* in this case. In their validation, Le Bars and Worster [17] neglected the advection term, allowing them to obtain results independent of *Pr*. In the present study, however, Eqs. (6)–(9) are solved without any further assumptions. Our results are therefore expected to depart from theirs with increasing *Ra*, indicating at the same time the increasing effect of advection.

Table 1
Comparison of *Nu* for a differentially heated porous cavity with uniform porosity – 81×81 grid, $Pr = 1.0$.

Da	*Ra*	$\epsilon = 0.4$			$\epsilon = 0.9$		
		Present study	[17]	[4]	Present study	[17]	[4]
10^{-6}	10^7	1.08	1.08	1.08	1.08	1.09	1.08
	10^8	3.07	3.07	2.99	3.08	3.08	3.01
	10^9	12.85	12.9	12.0	13.08	13.15	12.2
10^{-2}	10^3	1.01	1.01	1.02	1.02	1.02	1.02
	10^4	1.41	1.41	1.69	1.67	1.67	1.70
	10^5	3.17	3.17	3.80	4.09	4.09	4.19
	5×10^5	5.24	5.24	6.20	6.89	6.89	7.06

Table 2
Comparison of *Nu* for a differentially heated porous cavity – 81×81 grid, $Pr = 1.0$.

Da	*Ra*	Present study	[17]	[18]	[4]
10^{-6}	10^7	1.08	1.08	1.07	1.08
	10^8	3.10	3.08	3.06	3.004
	10^9	13.41	13.2	13.22	12.25
	5×10^9	31.7	30.9	31.50	–
10^{-4}	10^5	1.07	1.07	1.06	–
	10^6	2.86	2.85	2.84	–
	10^7	10.37	10.3	10.34	–
	5×10^7	20.56	20.1	20.85	–

4. Results and discussion

4.1. Flow description

This section describes the flow characteristics for both boundary conditions considered in this study.

4.1.1. Case A: left wall with a linear profile

The flow is characterized by a dominant anti-clockwise cell that starts at the upper part of the cavity at low *Ra* and extends to fill the entire cavity as *Ra* increases. For $A = 0.5$, a second cell forms in the hot lower corner due to the development of a temperature gradient in this area. For low *A* values, no secondary flow is apparent. Fig. 2 shows the streamlines and isotherms for the left and right half of the cavity respectively. At $Ra = 10^5$, the flow is weak and heat transfer is dominated by conduction, at $Ra = 10^6$, the flow is stronger and deformed isotherms show signs of convection onset. Convection regime is firmly established only at $Ra = 5 \times 10^6$ as seen from the meandering isotherms. A secondary, clockwise cell appears in the lower left corner of the cavity.

Fig. 2 is qualitatively identical to the results published in [13], which used finite-element approach, and confirms the validity of:

1. the finite-difference method adopted;
2. the implementation of the symmetry boundary condition permitting the use of half the computational domain.

The left side of Fig. 3 shows that part of the cavity is filled with calm, stratified medium, especially at lower $Ra \cdot Da$. The extent of the convective cell clearly increases as this product increases.

4.1.2. Case B: left wall with a sinusoidal profile

A sinusoidal cooling profile produces a two-cell pattern with competing behaviors. The upper cell behaves exactly as the main cell in Case A: the fluid loses energy to the surrounding walls and descends towards the middle of the cavity, where it starts to gain heat and consequently travels up the adiabatic boundary. The lower part of the cavity is occupied by a clockwise circulating cell, that increases in intensity as *Ra* increases. As a consequence of this flow pattern, no clear penetration length is established, as seen on the right of Fig. 3.

The two-cell pattern is reconfirmed in Fig. 4 for $Da = 10^{-6}$ and $A = 0.5$. A weak clockwise cell is present even at low *Ra* increasing in intensity to match the main anti- clockwise cell as *Ra* increases. Compared to Fig. 2, the sinusoidal temperature profile is clearly sufficient to maintain this multi-cellular pattern even for a moderate aspect ratio.

4.2. Heat transfer

Perhaps the most significant quantity for engineering applications is the overall *Nu* number or the ratio of convective to conductive heat transfer between a solid boundary and a moving fluid, defined here as:

$$Nu = \int_0^1 Nu_{loc} dy = \int_0^1 \frac{\partial \theta}{\partial x} dy \quad (13)$$

Nu plotted as a function of *Ra* (not shown) was found to agree with the results of Sathiyamoorthy et al. [13]. In order to understand the effect of the heating profile, the local distribution of the *Nu* number must also be investigated.

4.2.1. Case A

Fig. 5 shows the local Nu_{loc} distribution along the left wall. At low and moderate *Ra*, almost no heat is gained from the surround-

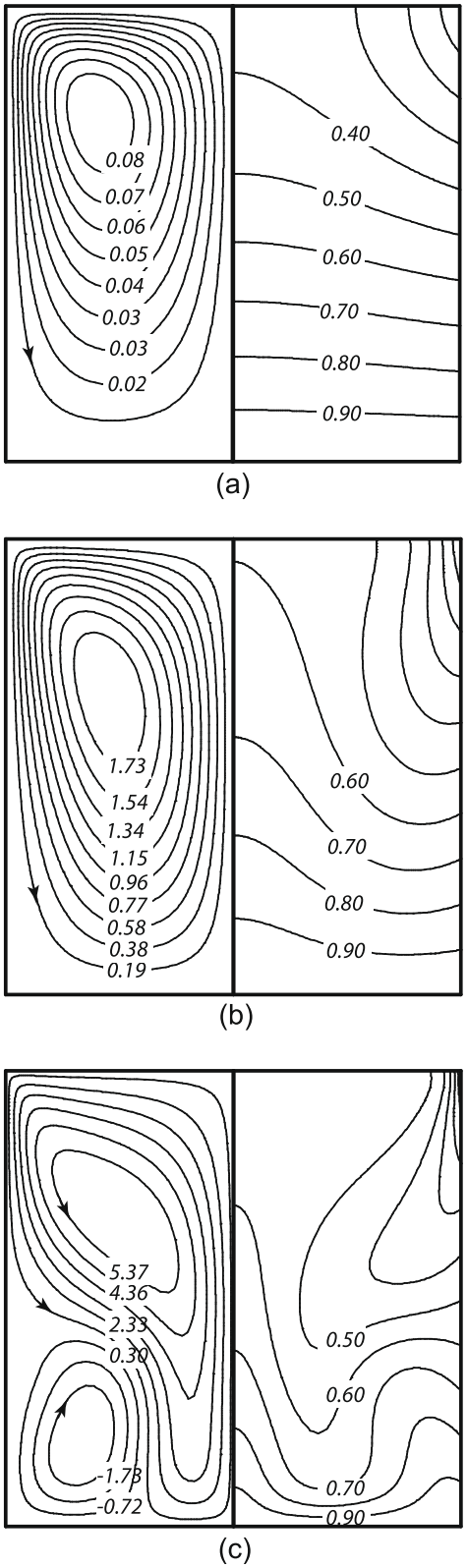

Fig. 2. Streamlines (left) and isotherms (right) for $Da = 10^{-4}$ and $A = 0.5$ cooled with linear profile. (a) $Ra = 10^5 (\psi_{max} = 0.085, \psi_{min} = 0.0)$, (b) $Ra = 10^6 (\psi_{max} = 1.920, \psi_{min} = 0.0)$, and (c) $Ra = 5 \times 10^6 (\psi_{max} = 6.386, \psi_{min} = -3.764)$.

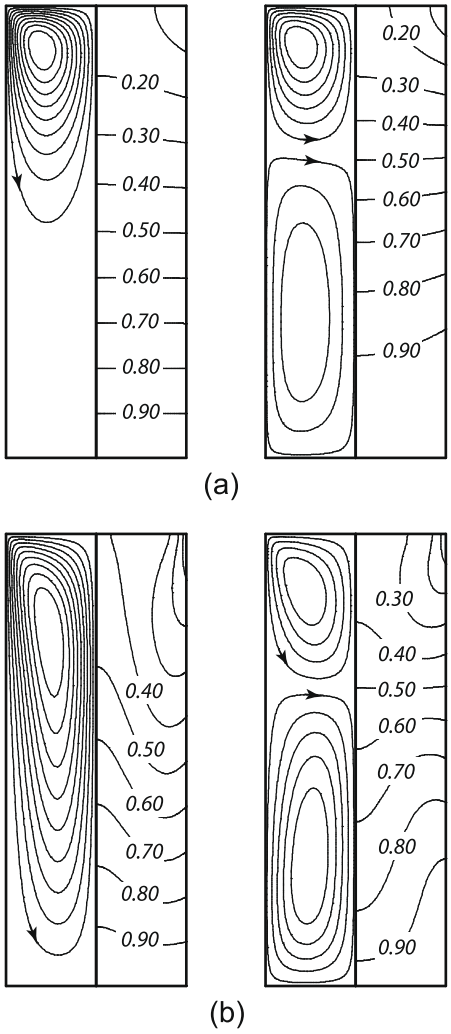

Fig. 3. Streamlines and isotherms for $Da = 10^{-6}$ and $A = 0.2$ cooled with linear (left) and sinusoidal (right) profiles. (a) $Ra = 10^8$, left $(\psi_{max} = 0.160, \psi_{min} = 0.0)$, right $(\psi_{max} = 0.227, \psi_{min} = -0.111)$ and (b) $Ra = 5 \times 10^8$, left $(\psi_{max} = 3.625, \psi_{min} = 0.0)$, right $(\psi_{max} = 2.018, \psi_{min} = -2.293)$.

ings for 80% of the cavity height, because the convective cell occupies only the upper part of the cavity. For the remaining 20%, heat is lost due to the temperature gradient between the hot porous media and the relatively cold wall. At higher *Ra*, heat is gained from the bottom part of the cavity and released to the upper part, giving a nearly constant value of *Nu* as a function of *Ra*, as can be seen from the area under the Nu_{loc} curve. Note that, for tall cavities, the point at which the cavity starts to lose heat to the surrounding walls ($Nu_{loc} < 0$) does not depend on *Ra*, and occurs at $y \approx 0.8$. With taller cavities ($A = 0.5$), multi-cellular flow occurs at high *Ra* and *Nu* distribution starts to show a wavy pattern (Fig. 6).

The overall *Nu* for two aspect ratios as a function of *Ra* is depicted in Fig. 7 where the *Nu* scale has been adjusted to account for the weaker heat transfer in tall cavities ($A = 0.2$). As expected, the onset of convection happens at higher *Ra* as *Da* decreases indicating a need for higher temperature gradient at lower permeability. It is interesting to note a slight inflection point happening towards the end of the conduction regime. It is more visible for taller cavity but can also be seen for $A = 0.5$ and was also reported elsewhere [13]. Further increase of *Ra* beyond this point firmly establishes the convection regime as it can be seen for $A = 0.5$. The overall heat transfer is lower for lower *A* due to a weaker convective cell in this case and to the presence of a stratified, motionless region. For instance, at $Da = 10^{-6}$, ψ_{max} and ψ_{min} equal 6.75 and -4.13 respectively for $A = 0.5$ and decrease (in absolute values) to $\psi_{max} = 3.625$ and $\psi_{min} = 0.0$ for $A = 0.2$.

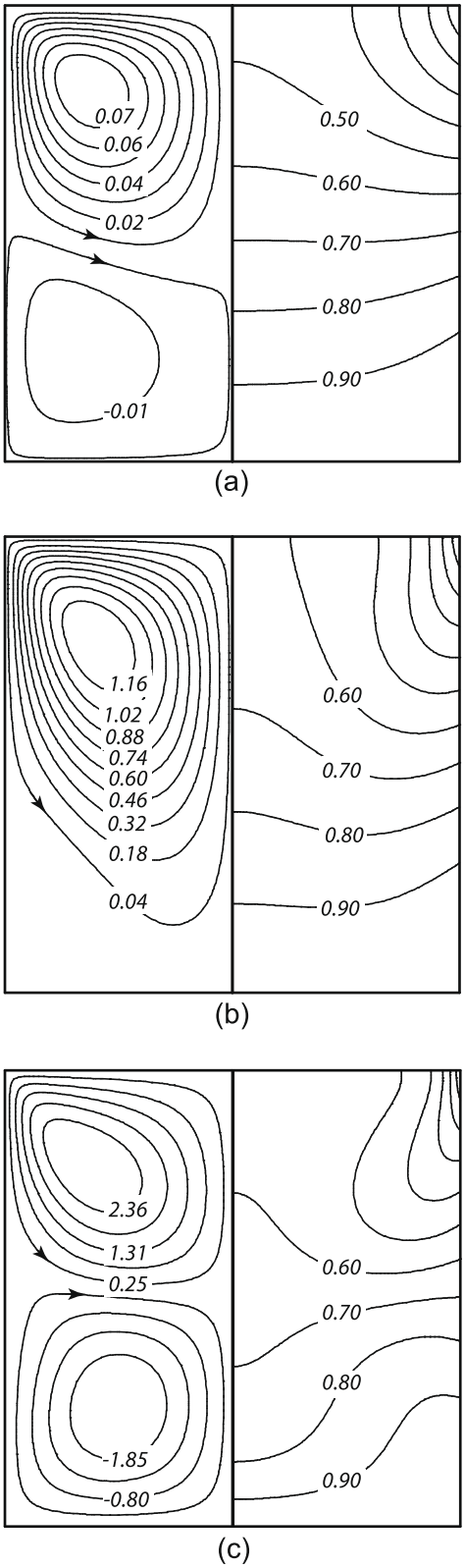

Fig. 4. Streamlines (left) and isotherms (right) for $Da = 10^{-4}$ and $A = 0.5$ cooled with sinusoidal profile. (a) $Ra = 10^5$ ($\psi_{max} = 0.076, \psi_{min} = -0.019$), (b) $Ra = 10^6$ ($\psi_{max} = 1.298, \psi_{min} = -0.099$) and (c) $Ra = 3 \times 10^6$ ($\psi_{max} = 2.890, \psi_{min} = -2.380$).

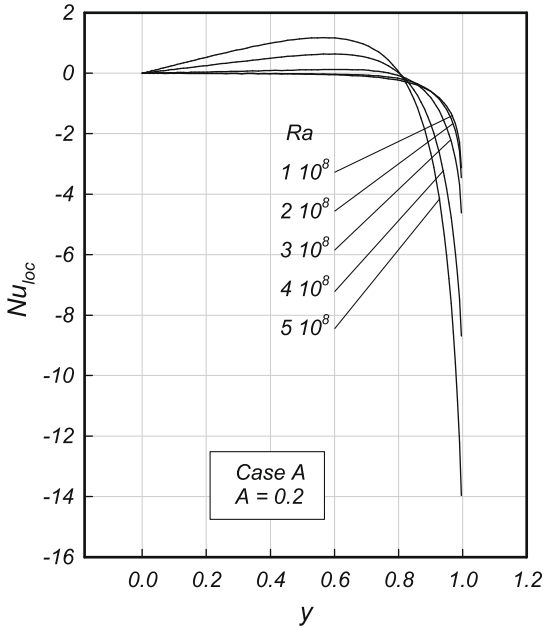

Fig. 5. Local Nusselt distribution along the left wall for a linear cooling profile. $Da = 10^{-6}$ and $A = 0.2$.

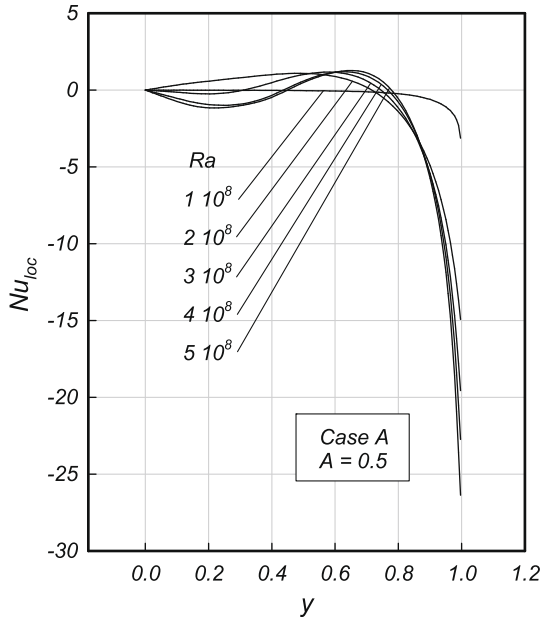

Fig. 6. Local Nusselt distribution along the left wall for a linear cooling profile. $Da = 10^{-6}$ and $A = 0.5$.

4.2.2. Case B

As opposed to Case *A* above, the Nu_{loc} distribution is no longer a two-pattern profile (see Fig. 8) due to the multi-cellular flow. The left wall can now be divided into four regions: starting from the bottom, heat is gained from the hot wall, causing a clockwise flow, the porous media then starts to lose heat to the surroundings. At the same time, a counter-clockwise cell occupying the top of the cavity loses heat at the top left corner, then starts to rise after receiving heat from the relatively hot wall.

Fig. 9 shows the *Nu* number for the sinusoidal profile as a function of *Ra*. The same observations as in case A are still valid except for $A = 0.2$. In the case of tall cavities, the sinusoidal profile promotes multi-cellular flow and enhances heat transfer by convection. In contrast, tall cavities with linear cooling profile exhibit a stagnated region with minimal heat transfer (see Fig. 3a).

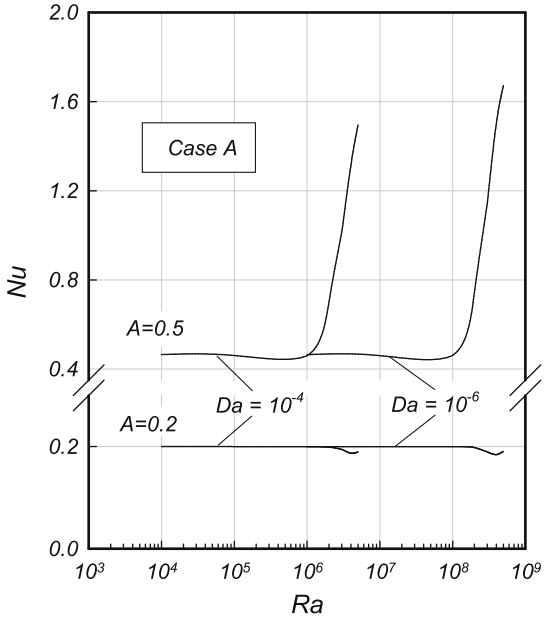

Fig. 7. Overall Nusselt on the left wall for a linear cooling profile as a function of *Ra* for $Da = 10^{-4}, Da = 10^{-6}$ and $A = 0.2, A = 0.5$.

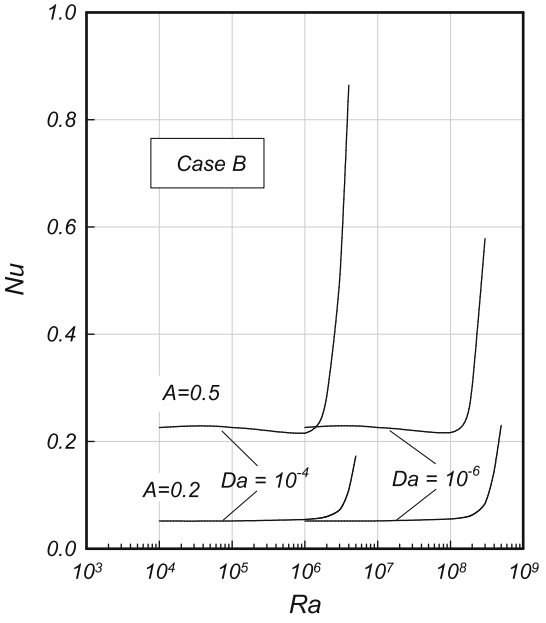

Fig. 9. Overall Nusselt on the left wall for a sinusoidal cooling profile as a function of *Ra* for $Da = 10^{-4}, Da = 10^{-6}$ and $A = 0.2, A = 0.5$.

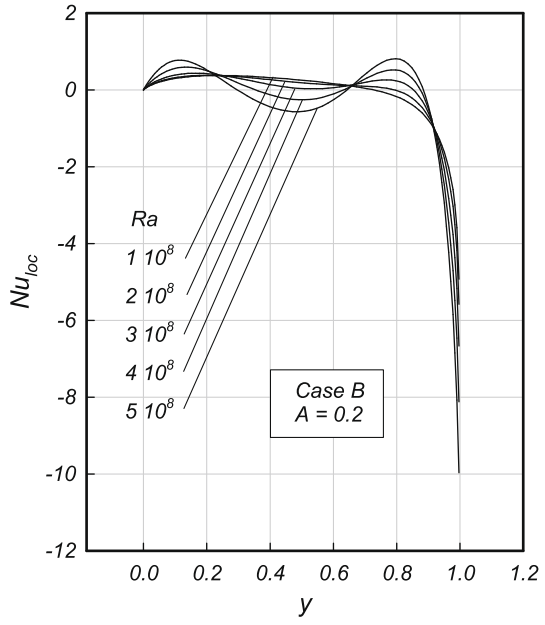

Fig. 8. Local Nusselt distribution along the left wall for a sinusoidal cooling profile. $Da = 10^{-6}$ and $A = 0.2$.

4.3. Scale analysis

From the above results, it appears that when the cavity is linearly cooled, the fluid in the bottom part stagnates so that only a portion of the cavity participates in the convection process. This behavior intensifies with increasing cavity height and decreasing *Ra*.

Let h_y represent the extent of the convective cell. h_y is much greater than the cavity width:

$$h_y \gg L \tag{14}$$

The pressure term is first eliminated from the governing Eqs. (2)–(5) by taking the derivative of the *x*-momentum and *y*-momentum equations and combining them. Considering Eq. (14) and further analysis of the order of magnitude of various terms in the conservation of mass, momentum, and energy leads to the following scales:

$$\frac{u'}{L} \sim \frac{v'}{h_y} \tag{15}$$

$$\frac{v'}{L} \sim \frac{Kg\beta}{\nu}\frac{\Delta T}{L} \tag{16}$$

$$u'\frac{\Delta T}{L} \sim \alpha\frac{\Delta T}{L^2} \tag{17}$$

Solving for h_y gives:

$$\frac{h_y}{H} \sim \left(\frac{L}{H}\right)^2 DaRa \tag{18}$$

Fig. 10 shows the velocity distribution on the right adiabatic plane (symmetry plane) as a function of *Ra*. The point where vertical velocity is less than a fraction of the maximum velocity (10% of v_{max}) is superimposed on the velocity plot, and is considered here to be a measure of the penetration length h_y.

The dots in Fig. 10 clearly show that this distance is linearly proportional to *Ra* at moderate *Rayleigh* numbers. When $Ra = 4 \times 10^8$, the convective cell covers the entire domain, for complete penetration. Beyond this state, further increase in *Ra* only increases the intensity of the convective cell or gives rise to secondary flow (Fig. 2c).

Fig. 11 shows the linear relation between penetration length and the *RaDa* product for a typical tall cavity ($A = 0.2$). The figure shows that the assumption is valid only for moderate *RaDa*, because for small values of this product, conduction is the dominant form of heat transfer and h_y takes an asymptotic value of about 0.5. The same is true for the high *RaDa* regime, where h_y departs from the plotted linear correlation due to the presence of a physical lower boundary that limits the extent of the convective cell, or in certain cases gives rise to multiple cells.

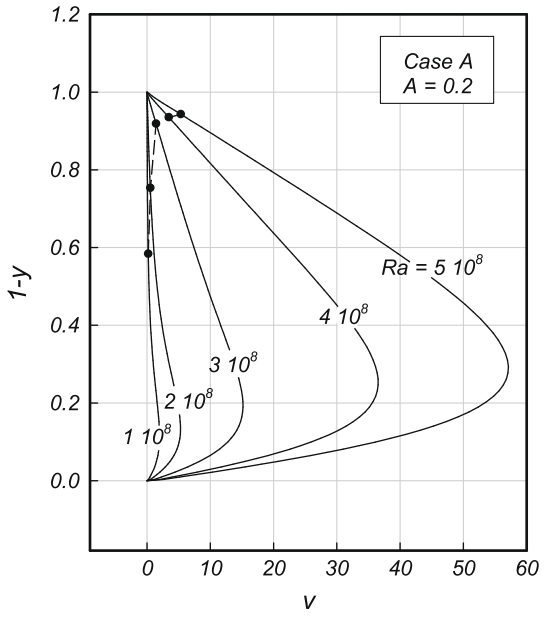

Fig. 10. Vertical velocity distribution on the symmetry plane as a function of $Ra, Da = 10^{-6}$.

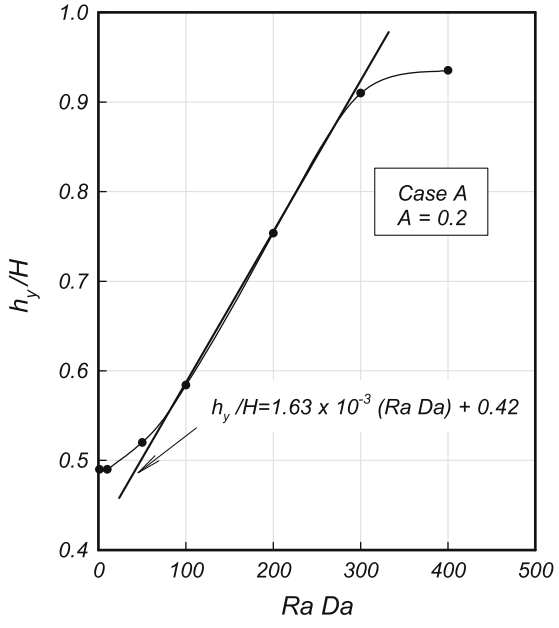

Fig. 11. Penetration length h_y as a function of *RaDa*.

5. Conclusion

A Darcy–Brinkman model is solved by a finite-difference method on half a rectangular cavity. Results are presented in terms of isotherm and streamline distribution and *Nu* profiles along the active wall at different *Ra* and *Da* numbers as well as aspect ratio *A*.

It appears that the flow is mostly unicellular when a linear profile is imposed (Case A), and a weak cell develops in the lower part of the cavity only at higher *Ra* with a nearly square cavity. In this case, scale analysis shows that the convective cell extent is proportional to both the *RaDa* product and the aspect ratio.

When a sinusoidal profile is imposed (Case B), the flow becomes bi-cellular, with clockwise circulation lower cell. These findings highlight the effect of boundary conditions on flow and heat transfer in tall cavities. Multi-cellular flow, and hence a wavy heat transfer pattern, is promoted by:

1. a sinusoidal temperature profile, in which the heating effect shifts towards the bottom wall;
2. lower aspect ratio (tall cavity).

References

[1] D.A. Nield, A. Bejan, Convection in Porous Media, Springer-Verlag, New York, 1999.
[2] K. Vafai, Handbook of Porous Media, second ed., Taylor & Francis, New York, 2005.
[3] K. Vafai, C.L. Tien, Boundary and inertia effects on flow and heat transfer in porous media, Int. J. Heat Mass Transfer 24 (1981) 195–203.
[4] P. Nithiarasu, K.N. Seetharamu, T. Sundararajan, Natural convective heat transfer in an enclosure filled with fluid saturated variable porosity medium, Int. J. Heat Mass Transfer 40 (1997) 3955–3967.
[5] I.A. Badruddin, Z.A. Zainal, P.A. Aswatha Narayana, K.N. Seetharamub, Numerical analysis of convection conduction and radiation using a non-equilibrium model in a square porous cavity, Int. J. Therm. Sci. 46 (2007) 20–29.
[6] W.J. Minkowycz, P. Cheng, Free convection about a vertical cylinder embedded in a porous medium, Int. J. Heat Mass Transfer 19 (1976) 805–813.
[7] R. Vasantha, G. Nath, Forced convection along a longitudinal cylinder embedded in a saturated porous medium, Int. Comm. Heat Mass Transfer 14 (1987) 639–646.
[8] A. Bejan, Natural convection in a vertical cylindrical well filled with porous medium, Int. J. Heat Mass Transfer 23 (1980) 726–729.
[9] A. Bejan, Convection Heat Transfer, Wiley Interscience Publication, 1984.
[10] O. Manca, S. Nardini, Experimental investigation on natural convection in horizontal channels with the upper wall at uniform heat flux, Int. J. Heat Mass Transfer 50 (2007) 1075–1086.
[11] E. Bilgen, R. Ben Yedder, Natural convection in enclosure with heating and cooling by sinusoidal temperature profiles on one side, Int. J. Heat Mass Transfer 50 (2007) 139–150.
[12] D. Poulikakos, Natural convection in a confined fluid-filled space driven by a single vertical wall with warm and cold regions, J. Heat Transfer 107 (1985) 867–876.
[13] M. Sathiyamoorthy, Tanmay Basak, S. Roy, I. Pop, Steady natural convection flow in a square cavity filled with a porous medium for linearly heated side wall(s), Int. J. Heat Mass Transfer 50 (2007) 1892–1901.
[14] S.V. Patankar, Numerical Heat Transfer and Fluid Flow, Hemisphere Publishing Corp., New York, 1980.
[15] R. Ben Yedder, Étude paramétrique de la convection laminaire et turbulente dans des espaces clos avec parois solides, Ph.D. Thesis, Université de Montréal, Canada, 1995.
[16] D. de Vahl Davis, Natural convection of air in a square cavity: a benchmark solution, Int. J. Num. Meth. Fluids 3 (1983) 249–264.
[17] M. Le Bars, M.G. Worster, Solidification of a binary alloy: finite-element, single-domain simulation and new benchmark solutions, J. Comput. Phys. 216 (2006) 247–263.
[18] G. Lauriat, V. Prasad, Non-Darcian effects on natural convection in a vertical porous enclosure, Int. J. Heat Mass Transfer 32 (1989) 2135–2148.